Clim. Past Discuss., 11, 1795–1820, 2015
www.clim-past-discuss.net/11/1795/2015/
doi:10.5194/cpd-11-1795-2015

Climate of the Past
Discussions
Open Access

Frequency, magnitude and character of hyperthermal events at the onset of the Early Eocene Climatic Optimum

V. Lauretano[1], K. Littler[2,*], M. Polling[1], J. C. Zachos[2], and L. J. Lourens[1]

[1]Department of Earth Sciences, Faculty of Geosciences, Utrecht University, Heidelberglaan 2, 3584CS, Utrecht, the Netherlands
[2]Department of Earth and Planetary Sciences, University of California Santa Cruz, 1156 High Street, Santa Cruz, CA 95064, USA
[*]now at: Camborne School of Mines, University of Exeter, Penryn Campus, Penryn, Cornwall, TR10 9FE, UK

Received: 20 April 2015 – Accepted: 21 April 2015 – Published: 13 May 2015

Correspondence to: V. Lauretano (v.lauretano@uu.nl)

Published by Copernicus Publications on behalf of the European Geosciences Union.

Abstract

Recent studies have shown that the Early Eocene Climatic Optimum (EECO) was preceded by a series of short-lived global warming events, known as hyperthermals. Here we present high-resolution benthic stable carbon and oxygen isotope records from ODP Sites 1262 and 1263 (Walvis Ridge, SE Atlantic) between ~ 54 and ~ 52 million years ago, tightly constraining the character, timing, and magnitude of six prominent hyperthermal events. These events, that include Eocene Thermal Maximum (ETM) 2 and 3, are studied in relation to orbital forcing and long-term trends. Our findings reveal an almost linear relationship between $\delta^{13}C$ and $\delta^{18}O$ for all these hyperthermals, indicating that the eccentricity-paced co-variance between extreme perturbations in the exogenic carbon pool and deep-sea temperatures persisted during the onset of the EECO, in accord with previous observations for the Paleocene Eocene Thermal Maximum (PETM) and ETM2. The covariance of $\delta^{13}C$ and $\delta^{18}O$ during H2 and I2, which are the second pulses of the "paired" hyperthermal events ETM2-H2 and I1-I2, deviates with respect to the other events. This could relate to a relatively higher contribution of an isotopically heavier source of carbon, such as peat or permafrost, and/or to climate feedbacks/local changes in circulation. Finally, the $\delta^{18}O$ records of the two sites show a systematic offset with on average 0.2 ‰ heavier values for the shallower Site 1263, which we link to a slightly heavier (e.g. more saline) isotope composition of the intermediate water mass reaching the northeastern flank of the Walvis Ridge compared to that of the deeper northwestern water mass at Site 1262.

1 Introduction

The early Paleogene was characterized by a highly dynamic climatic system both on long- (> 10^6 years) and short- (< 10^4 years) time scales. From the Late Paleocene (~ 58 Ma) to the Early Eocene (~ 50 Ma), Earth's surface experienced a long-term warming trend, resulting in an increase of at least 5 °C in deep ocean temperature

CPD
11, 1795–1820, 2015

Frequency, magnitude and character of hyperthermal events

V. Lauretano et al.

and an extended period of extreme warmth, called the Early Eocene Climatic Optimum (EECO, ~ 50–52 Ma; Zachos et al., 2001, 2008; Bijl et al., 2009; Westerhold and Röhl, 2009). Superimposed on this warming trend were a series of short-lived global warming (hyperthermal) events, driven by the release of ^{13}C-depleted carbon into the ocean–atmosphere carbon reservoirs (Zachos et al., 2005; Lourens et al., 2005; Nicolo et al., 2007; Littler et al., 2014; Kirtland Turner et al., 2014). These events are of particular interest as they represent useful key-analogs for the current global warming, despite differences in background climatic conditions (e.g., Zachos et al., 2008; Hönisch et al., 2012; Zeebe and Zachos, 2013).

The Paleocene Eocene Thermal Maximum (PETM or ETM1, ~ 56 Ma), lasting less than 200 kyr, was the most extreme of these episodes. During the PETM global temperature raised by 5–8 °C, resulting from a massive carbon release as evidenced by a significant negative carbon isotope excursion (CIE) of > 3 ‰ in the ocean/atmosphere carbon pools, and widespread dissolution of seafloor carbonate (Kennett and Stott, 1991; Dickens et al., 1995; Thomas and Shackleton, 1996; Zachos et al., 2005, 2008; Sluijs et al., 2007; McInerney and Wing, 2011). A series of similar events are recorded in carbonate records from marine and continental deposits from the early Paleogene and expressed by negative excursions in δ^{13}C and δ^{18}O as well as dissolution horizons (e.g., Cramer et al., 2003; Lourens et al., 2005; Agnini et al., 2009; Galeotti et al., 2010; Stap et al., 2010; Zachos et al., 2010; Abels et al., 2012, 2015; Slotnick et al., 2012; Kirtland Turner et al., 2014; Littler et al., 2014). Orbitally-tuned records for this geological interval provide evidence that the occurrence of the early Eocene hyperthermal events was paced by variations in the Earth's orbit, specifically in the long and short eccentricity cycles. (e.g., Cramer et al., 2003; Lourens et al., 2005; Littler et al., 2014; Zachos et al., 2010; Sexton et al., 2011).

Several different carbon sources have been proposed to explain the negative CIE, including: (1) the release of methane by thermal dissociation of gas hydrates on the continental slopes (Dickens et al., 1995), (2) the burning of peat and coal deposits (Kurtz et al., 2003); and (3) the release of carbon from thawing of permafrost soils at

CPD
11, 1795–1820, 2015

high latitudes as a feedback or as a direct response to orbital forcing (DeConto et al., 2012); while (4) a redistribution of ^{13}C-depleted carbon within oceans has been proposed as mechanism for hyperthermals in the Early to Middle Eocene interval (Sexton et al., 2011).

Despite the uncertainty in carbon source and triggering mechanism of the hyperthermal events, a common reservoir has been theorized to explain the consistent covariance in benthic foraminiferal $\delta^{13}C$ and $\delta^{18}O$ across both the PETM and ETM2, indicating that changes in the exogenic carbon pool were similarly related to warming during these events (Stap et al., 2010). The aim of this paper is to test this relationship by constraining the relative timing and magnitude of changes in deep ocean temperatures and carbon isotope excursions for a series of carbon isotope excursions that succeed ETM2, initially identified by Cramer et al. (2003) in the composite bulk carbonate $\delta^{13}C$ record from several deep-sea sites (ODP Sites 690 and 1051; DSDP Site 550 and 577). For this purpose, we generated high-resolution carbon and oxygen stable isotope records of the benthic foraminiferal species *Nuttalides truempyi* of ODP Sites 1262 and 1263 (Walvis Ridge) encompassing the interval from the ETM2 (Stap et al., 2010) to the ETM3 (Röhl et al., 2005), providing the first complete high-resolution benthic stable isotope records for the Early Eocene events leading to the EECO.

2 Materials and methods

2.1 Site location and sampling

ODP Sites 1262 and 1263 represent the deepest and shallowest end-member of a 2 km depth transect recovered during ODP Leg 208. Site 1263 is located just below the crest of the northeast flank of Walvis Ridge, in the southeastern Atlantic, at a water depth of 2717 m, whereas Site 1262 was drilled near the base of the northwestern flank of Walvis Ridge at a water depth of 4759 m (Fig. 1). The estimated paleodepth of Sites 1262 and 1263 at ~ 56 Ma were ~ 3600 and 1500 m, respectively (Zachos et al., 2004).

CPD
11, 1795–1820, 2015

The material recovered at the two sites provided an expanded sequence of early Paleogene sediments, yielding a complete section mainly composed of calcareous nannofossil ooze, chalk and marls. The relatively shallow depth of Site 1263 promoted uninterrupted deposition of carbonate-rich sediments, as it remained well above the lysocline throughout the Paleogene. The composite depth scale for Site 1263 was constructed using the magnetic susceptibility (MS) and sediment lightness (L*) from the four holes (Zachos et al., 2004).

Samples were collected at the Bremen Core Repository from Holes A, B and C for Site 1263, and Holes A and B for Site 1262, according to the shipboard meters composite depth section (mcd) (Zachos et al., 2004). A 28 m thick interval of Site 1263 was sampled at a resolution of 5 cm from ∼ 268 to ∼ 296 mcd, and a ∼ 6 m interval of Site 1262 was sampled at a resolution of 3 cm from ∼ 103 to ∼ 109 mcd. Prior to the analyses, samples were freeze dried, washed and sieved to obtain fractions larger than 38, 63 and 150 µm at University of California, Santa Cruz and Utrecht University.

2.2 Stable isotopes

Multi-specimen samples of *N. truempyi* were picked from the > 150 µm fraction. Stable isotopes analyses of Site 1263 were carried out at Utrecht University on an average of 6–8 foraminiferal calcite tests using a CARBO-KIEL automated carbonate preparation device linked on-line to a Thermo-Finnigan MAT253 mass spectrometer. Calibrations to the international standard (NBS-19) and to the in-house standard (Naxos marble) show an analytical precision of 0.03 and 0.08 ‰ for δ^{13}C and δ^{18}O, respectively. Picked specimens from Site 1262 were analyzed on a KIEL IV carbonate preparation device linked on-line to a Thermo-Finnigan MAT253 mass spectrometer, at the UCSC Stable Isotope Laboratory, Santa Cruz. Calibration to the in-house standard Carrara marble (CM05) and international standards (NBS-18 and NBS-19) revealed an analytical precision of 0.05 and 0.08 ‰, for δ^{13}C and δ^{18}O, respectively. All values are reported in standard delta notation relative to VPDB (Vienna Pee Dee Belemnite). Outliers were defined by adding or subtracting an upper and lower boundary of 2σ from a 13-points

CPD
11, 1795–1820, 2015

moving average, following the method by Liebrand et al. (2011). Published benthic isotope data of the same foraminiferal species for the ETM2 (or H1/Elmo event) and H2 were included in this study to obtain a longer continuous record of Site 1263 and 1262 (Stap et al., 2010) and for I1-I2 of Site 1262 (Littler et al., 2014).

2.3 Paleotemperature reconstructions

Paleotemperatures were obtained from the δ^{18}O values by applying the equation of Bemis et al. (1998):

$$T\ (°\mathrm{C}) = 16.9 - 4.38\left(\delta^{18}\mathrm{O_c} - \delta^{18}\mathrm{O_{sw}}\right) + 0.10\left(\delta^{18}\mathrm{O_c} - \delta^{18}\mathrm{O_{sw}}\right)^2 \quad (1)$$

where the value for $\delta^{18}\mathrm{O_{sw}}$ was corrected from SMOW to PDB scales by subtracting 0.27 ‰ (Hut, 1987). The *N. truempyi* δ^{18}O was corrected for seawater equilibrium by adding 0.35 ‰ (Shackleton and Hall, 1997).

3 Age model

Given the typical low resolution age control afforded by magneto- and bio-stratigraphy, and the availability of a robust cycle (i.e., orbital) based chronology for the Leg 208 sites (Westerhold et al., 2007), we developed an eccentricity-tuned age model for the studied interval using the red over green color ratio (a*) records of ODP Sites 1263 and 1262 (Fig. 2). For tuning, we applied first spectral analysis in the depth domain using standard Blackman–Tukey and Gaussian filtering techniques as provided by the AnalySeries program (Paillard et al., 1996). Site 1262, the deepest site at Walvis Ridge, was chosen as the backbone for our tuning. The a* record of this site clearly revealed a ∼ 3 m period, interpreted as reflecting the climatic imprint of the 405 kyr eccentricity cycle (Lourens et al., 2005). Subsequently, we filtered this component and tuned it directly to the extracted 405 kyr eccentricity component of the La2010d orbital solution

CPD
11, 1795–1820, 2015

(Laskar et al., 2011) with maximum a* values corresponding to maximum eccentricity values (Table 1). A similar approach was carried out for the a* record of Site 1263 to evaluate the continuity of the successions and robustness of the filtered output (Fig. 2). Finally, the tuned age model of Site 1262 was transferred to Site 1263 by correlating > 50 characteristic features in the a* records of both sites as tie points (Fig. 2 and Table 2).

Different tuning options have been debated in the last 10 years, resulting in an age for the PETM ranging between ~ 55.5 and ~ 56.3 My (Lourens et al., 2005; Westerhold et al., 2008; Hilgen et al., 2010; Dinarès-Turell et al., 2014). Here we report on two tuning options (Fig. 2), assigning an age of 53.69 ± 0.02 (option 1) or of 54.09 ± 0.02 (option 2) to ETM2 (Westerhold et al., 2007). According to both options, ETM2 predates the 405 kyr maximum falling at an increasing limb, in agreement with observations of Westerhold et al. (2007), but in contrast with the earlier interpretation by Lourens et al. (2005), who aligned this event to a maximum in the 405 kyr cycle. Recent literature revising the Paleocene cyclostratigraphic interpretation (Dinarès-Turell et al., 2014; Hilgen et al., 2015) have shown that the Paleocene holds 25 rather than 24 × 405 kyr eccentricity cycles. In addition, new U/Pb ages have become available which support an age of ~ 66.0 Ma for the K/Pg boundary (Kuiper et al., 2008; Renne et al., 2013). These developments point to an age of ~ 54.0 Ma for ETM2 and therefore we plot our results anchoring the age of ETM2 to option 2 (Fig. 3). Evolutionary wavelet spectra were obtained in the time domain using the wavelet script of Torrence and Compo (http://paos.colorado.edu/research/wavelets). Prior to the analysis, carbon and oxygen records were resampled at 2.5 kyrs, detrended and normalized.

4 Results

Our new benthic $\delta^{13}C$ and $\delta^{18}O$ records show six major negative excursions between 54 and 52 Ma (Fig. 3). They correspond to the ETM2, H2, I1, I2, J, and ETM3/X/K events, formerly recognized in deep-sea $\delta^{13}C$ bulk carbonate records and land-based

CPD
11, 1795–1820, 2015

marine and continental sections (Cramer et al., 2003; Lourens et al., 2005; Agnini et al., 2009; Slotnick et al., 2012; Abels et al., 2012, 2015; Kirtland Turner et al., 2014; Littler et al., 2014).

The general long-term trend in our ~ 2 Ma long records indicates a minor increase between 54.2 and 53.2 Ma followed by an average decrease of ~ 0.3 ‰ in absolute values of both δ^{13}C and δ^{18}O baseline values following J (~ 53.1 Ma), with minor cycles evident between the six main events in both records. Following J, both records maintain rather stable values up to ETM3 (Fig. 3). Both these changes are negligible compared to the Paleocene–Eocene long–term warming trend and long-term negative trend in carbon isotope values. However, the onset of more generally negative δ^{13}C values, coinciding with J, has also been observed in the deep-sea bulk carbonate record at Site 1262 (Zachos et al., 2010) and in the land-based section at Mead Stream by Slotnick et al. (2012), who suggested that it might be used to mark the onset of the EECO.

The onset of warmer temperatures leading to the EECO is evident at ~ 53 Ma in the benthic δ^{18}O records at both Sites 1262 and 1263 (Fig. 3). Baseline average δ^{18}O values prior to ETM2, representing the response of the unperturbed oceanic system, represent a mean deep-sea temperature of ~ 12 °C, which post-J increases by > 0.5 °C. On the short-term scale, our new data across the events following ETM2 and H2 indicate a rise in temperature of ~ 2 and ~ 1.5 °C during I1 and I2, respectively. The event labelled as J was associated with a temperature increase of > 1 °C superimposed on the further average decrease in baseline δ^{18}O values. The ETM3 is expressed in both the shallowest and deepest site at Walvis Ridge by similar isotopic excursions with a CIE of ~ 0.8 ‰ and a shift in the oxygen record of ~ 0.5 ‰, corresponding to a warming in the deep ocean of 2–2.5 °C, comparable to values observed during the ETM2 (Stap et al., 2010).

Evolutionary wavelet analyses for δ^{13}C and δ^{18}O records of Site 1263 show spectral power concentrated at distinct frequencies, corresponding to the long 405 kyr and short ~ 100 kyr eccentricity cycles (Fig. 4). The isotope records reveal coherent patterns, with the highest spectral power concentrated during the ETM2–H2 and I1–I2. The ~ 100 kyr

CPD
11, 1795–1820, 2015

signal in δ^{13}C, which is very prominent in the first 1 Ma of the record, weakens after J. The imprint of precession and/or obliquity forcing is very weak/absent throughout the entire record. As a result of our tuning approach, minima in δ^{13}C are approximately in phase with maxima in the 405 and ~ 100 kyr eccentricity cycles, following previous work (e.g., Cramer et al., 2003; Lourens et al., 2005; Zachos et al., 2010; Stap et al., 2010).

5 Discussion

5.1 Isotope covariance

The coherent response between benthic δ^{13}C and δ^{18}O implies a strong relationship between changes in the carbon cycle and climate throughout the interval, as has been observed in the older part of the record at Site 1262 (Stap et al., 2010; Littler et al., 2014). The covariance and cyclicity evident in the isotopic records suggest a strong non-linear response to orbital forcing, leading to the release of isotopically-light carbon (e.g. methane gas and/or CO_2) to the ocean–atmosphere system during eccentricity maxima, driving subsequent carbonate dissolution and warming. It has been theorized that the timing and magnitude would respond to the crossing of a thermal threshold, more frequently reached in phases of orbitally-driven temperature increase (Lunt et al., 2011). Consequently, the carbon reservoir, regardless of its nature, would reach the complete depletion across the EECO to then progressively fill again, leading to a specular series of global warming events of decreasing frequency and increased size along the post-EECO cooling phase and an interval free of hyperthermals during the peak of the EECO (Kirtland Turner et al., 2014). However, δ^{13}C data from a composite stable isotope record have disproved this hypothesis showing that episodes of carbon release continued throughout the EECO and the onset of the cooling trend. This evidence suggests that mechanisms similar to those invoked for the Oligocene and Miocene were controlling the Eocene climate (Kirtland Turner et al., 2014). Our benthic isotope

CPD
11, 1795–1820, 2015

records support this hypothesis and allow for a direct test of the temperature related signal carried by the benthic foraminiferal $\delta^{18}O$ for the hyperthermals leading to the EECO. The six events recognised in the benthic record of Site 1263 vary in terms of both the magnitude of the CIEs and the inferred temperature changes. The most intense perturbations are associated with the ETM2, I1 and ETM3, whereas H2 and I2, which lag the larger events by one 100 kyr eccentricity period, are less prominent (Fig. 3). One important question is whether all these events of varying magnitude share the same underlying mechanism, in terms of the source of light carbon to the ocean atmosphere system and climatic response. Following Stap et al. (2010), we have assessed this by comparing the slopes of the regression line between the carbon and oxygen isotopes of the individual events (Fig. 5). These cross-plots clearly show that all events exhibit significant and coherent linear relationships between both sites with slopes ranging between 0.5 and 0.7 (Fig. 5), suggesting a constant ratio of temperature response to input of carbon release.

The slopes of the regression lines for H2 and I2 appear slightly steeper than those of ETM2, I1, J and ETM3 (Fig. 5). To statistically test this (dis)similarity, we applied a student *t* test to pairs of slopes, comparing all the events against each other using both a pooled and an unpooled error variance. The results show that the null hypothesis (the slopes being similar, $\alpha = 0.05$) is satisfied in the case of ETM2, I1, J and ETM3. The tests on the steeper slopes of H2 and I2 generally display values of $p \leq 0.05$ when tested against the other events, but values of $p \geq 0.05$ when tested against each other. This implies that the H2 and I2 show to be statically similar to each other but to slightly differ from the remaining events. Even though this statistical approach might be subject to limitations derived from the range of data points chosen for each event, it clearly shows that the slopes for H2 and I2 deviate from the average values given by the other events. Moreover, the statistical deviation of the slopes of H2 and I2 is clearer when comparing them with the average slope for all events of the two sites, since they fall outside the (99.99 %) confidence limits (Fig. 6). The average slope between

CPD
11, 1795–1820, 2015

$\delta^{13}C$ and $\delta^{18}O$ of 0.6 for both sites is also in accord with previous observations for the onset/recovery of PETM, ETM2 and H2 by Stap et al. (2010).

The "paired" hyperthermal events, ETM2–H2 and I1–I2 thus reveal slightly different $\delta^{13}C$ vs. $\delta^{18}O$ relationships between their first (ETM2 and I1) and secondary (H2 and I2) pulses. Assuming that these signals are globally representative, this could imply that the second of the two pulses had a relatively larger contribution of an isotopic heavier carbon source than the first pulse. Such a mechanism could hint to a methane-related dominant carbon source (e.g. methane hydrates) during the initial phase of the paired hyperthermal events, whereas other relatively heavier carbon isotope sources (e.g. wetlands, peat) might have become progressively more important during the successive phase. This mechanism could be linked to the depletion and subsequent recharge time of the inferred methane clathrate reservoir between both events. If this is true, however, we might expect that the amount of carbonate dissolution associated with the shoaling of the calcite compensation depth (CCD) and lysocline during these two pulses were more or less similar. Evidently, the a* values, representative of redness and hence carbonate dissolution, were significantly lower during the second pulses than during their preceding counterparts (Fig. 2). This suggests that local circulation changes or partial dissolution may have slightly altered the anomalies in $\delta^{18}O$ and $\delta^{13}C$ during H2 and I2. Assuming climate sensitivity to be constant, global temperatures would respond non-linearly to increasing $p CO_2$. However, our results show that the temperature response to episodes of carbon release appears to be linear during this time interval. This may also suggest that climate feedbacks or an incomplete recovery of the buffering capacity of the ocean system after the first perturbation could have played a significant role in amplifying the temperature response observed in our data. However, the scaling of CIE magnitudes between deep-sea and continental records for these events indicates an approximately scaled relationship, strengthening the hypothesis of a similar isotopic composition of the carbon source for the early Eocene hyperthermal events (Abels et al., 2015).

CPD
11, 1795–1820, 2015

In this respect it is worth noting that these latter two events also behave differently from the "larger" events in terms of biotic disruption (Gibbs et al., 2012). While for PETM, ETM2 and I1, data indicate a scaled biotic response to carbon injections, in the cases of H2 and I2 the system apparently failed to cross the environmental "threshold" necessary to generate a detectable marine biotic disruption (D'haenens et al., 2012; Gibbs et al., 2012).

5.2 Site 1263 vs. Site 1262

Comparison between the benthic $\delta^{13}C$ and $\delta^{18}O$ records of Sites 1263 and 1262 reveals an almost identical pattern, although $\delta^{18}O$ values of Site 1263 are consistently ~ 0.2 ‰ heavier than those of Site 1262 (Fig. 3). A similar (reversed) pattern has been previously observed by Stap et al. (2009) in the case of ETM2, where it was attributed to differential dissolution from the shallowest to the deepest site. Conversely, selective dissolution seems unlikely to justify the persistent offset in $\delta^{18}O$ values observed throughout the new post-ETM2 record presented herein. This offset cannot be explained by a temperature-dependence, since Site 1262 is bathed by a deeper, and hence colder, water mass than the shallower Site 1263. Therefore, we link this offset to a difference in the average isotopic composition of the water masses at those sites. Accordingly, this suggests the intermediate water mass reaching Site 1263 was more ^{18}O-enriched than the deeper waters at Site 1262, and more saline.

6 Conclusions

The new high-resolution benthic stable isotope records from ODP Sites 1262 and 1263 provide a detailed framework to explore the nature of Early Eocene hyperthermal events. Our results in the interval from ETM2 to ETM3 confirm the link between large-scale carbon emissions and climate response to orbital forcing, in particular to short- and long- eccentricity cycles. The transition towards the Early Eocene Climatic

Optimum is marked by a general decrease of both benthic carbon and oxygen isotopic values of ~ 0.3 ‰ at Site 1263, indicative of both long-term warming and progressive release of organic carbon into the ocean–atmosphere system. Consistent covariance between benthic carbon and oxygen isotopes during each of the studied events suggests a constant temperature response to changes in the exogenic carbon pool. However, the second of the hyperthermal events occurring in "pairs" during times of 405 kyr eccentricity maxima (H2 and I2) point to a slightly different behaviour. Whether this implies a larger role for a carbon reservoir characterized by a heavier isotopic signature remains debatable and, hence, allows for further considerations about other operational processes like local circulation changes, partial dissolution, or different climate feedbacks.

Finally, an offset in oxygen isotopic values between Site 1263 and 1262, with the latter consistently heavier than the former, suggests that more saline intermediate waters reached the shallowest site of the Walvis Ridge transect, providing new information about the water column structure of the ancient South Atlantic Ocean.

Acknowledgements. We thank the International Ocean Discovery Program (IODP) for providing the samples used in this study. We also thank A. van Dijk at Utrecht University, and Dyke Andreasen and Chih-Ting Hsieh at UCSC for analytical support. This research was funded by NWO-ALW grant (project number 865.10.001) to L. J. Lourens. We thank F. Hilgen and H. A. Abels for providing valuable comments on the manuscript.

References

Abels, H. A., Clyde, W. C., Gingerich, P. D., Hilgen, F. J., Fricke, H. C., Bowen, G. J., and Lourens, L. J.: Terrestrial carbon isotope excursions and biotic change during Palaeogene hyperthermals, Nat. Geosci., 5, 326–329, doi:10.1038/ngeo1427, 2012.

Abels, H. A., Lauretano, V., van Yperen, A., Hopman, T., Zachos, J. C, Lourens, L. J., Gingerich, P. D., Bowen, G. J.: Carbon isotope excursions in paleosol carbonate marking five early Eocene hyperthermals in the Bighorn Basin, Wyoming, Clim. Past Discuss., accepted, 2015.

CPD
11, 1795–1820, 2015

Frequency, magnitude and character of hyperthermal events

V. Lauretano et al.

Title Page
Abstract | Introduction
Conclusions | References
Tables | Figures
◂ | ▸
Back | Close
Full Screen / Esc
Printer-friendly Version
Interactive Discussion

Agnini, C., Macri, P., Backman, J., Brinkhuis, H., Fornaciari, E., Giusberti, L., Luciani, V., Rio, D., Sluijs, A., and Speranza, F.: An early Eocene carbon cycle perturbation at ∼ 52.5 Ma in the Southern Alps: chronology and biotic response, Paleoceanography, 24, PA2209, doi:10.1029/2008PA001649, 2009.

Bemis, B. E., Spero, H. J., Bijma, J., and Lea, D. W.: Reevaluation of the oxygen isotopic composition of planktonic foraminifera: experimental results and revised paleotemperature equations, Paleoceanography, 13, 150–160, 1998.

Bijl, P. K., Schouten, S., Sluijs, A., Reichart, G.-J., Zachos, J. C., and Brinkhuis, H.: Early Palaeogene temperature evolution of the southwest Pacific Ocean, Nature, 461, 776–779, doi:10.1038/nature08399, 2009.

Cramer, B. S., Wright, J. D., Kent, D. V., and Aubry, M.-P.: Orbital climate forcing of δ^{13}C excursions in the late Paleocene–early Eocene (chrons C24n–C25n), Paleoceanography, 18, 1097, doi:10.1029/2003PA000909, 2003.

D'haenens, S., Bornemann, A., Stassen, P., and Speijer, R. P.: Multiple early Eocene benthic foraminiferal assemblage and δ^{13}C fluctuations at DSDP Site 401 (Bay of Biscay – NE Atlantic), Mar. Micropaleontol., 88–89, 15–35, doi:10.1016/j.marmicro.2012.02.006, 2012.

DeConto, R. M., Galeotti, S., Pagani, M., Tracy, D., Schaefer, K., Zhang, T., Pollard, D., and Beerling, D. J.: Past extreme warming events linked to massive carbon release from thawing permafrost, Nature, 484, 87–91, doi:10.1038/nature10929, 2012.

Dickens, G. R., O'Neil, J. R., Rea, D. K., and Owen, R. M.: Dissociation of oceanic methane hydrate as a cause of the carbon isotope excursion at the end of the Paleocene, Paleoceanography, 10, 965–971, 1995.

Dinarès-Turell, J., Westerhold, T., Pujalte, V., Röhl, U., and Kroon, D.: Astronomical calibration of the Danian stage (Early Paleocene) revisited: settling chronologies of sedimentary records across the Atlantic and Pacific Oceans, Earth Planet. Sc. Lett., 405, 119–131, doi:10.1016/j.epsl.2014.08.027, 2014.

Galeotti, S., Krishnan, S., Pagani, M., Lanci, L., Gaudio, A., Zachos, J. C., Monechi, S., Morelli, G., and Lourens, L. J.: Orbital chronology of Early Eocene hyperthermals from the Contessa Road section, central Italy, Earth Planet. Sc. Lett., 290, 192–200, doi:10.1016/j.epsl.2009.12.021, 2010.

Gibbs, S. J., Bown, P. R., Murphy, B. H., Sluijs, A., Edgar, K. M., Pälike, H., Bolton, C. T., and Zachos, J. C.: Scaled biotic disruption during early Eocene global warming events, Biogeosciences, 9, 4679–4688, doi:10.5194/bg-9-4679-2012, 2012.

CPD
11, 1795–1820, 2015

Frequency, magnitude and character of hyperthermal events

V. Lauretano et al.

Hilgen, F. J., Kuiper, K. F., and Lourens, L. J.: Evaluation of the astronomical time scale for the Paleocene and earliest Eocene, Earth Planet. Sc. Lett., 300, 139–151, doi:10.1016/j.epsl.2010.09.044, 2010.

Hilgen, F. J., Abels, H. A., Kuiper, K. F., Lourens, L. J., and Wolthers, M.: Towards a stable astronomical time scale for the Paleocene: aligning Shatsky Rise with the Zumaia – Walvis Ridge ODP Site 1262 composite, Newsl. Stratigr., 48, 91–110, doi:10.1127/nos/2014/0054, 2015.

Hönisch, B., Ridgwell, A., Schmidt, D. N., Thomas, E., Gibbs, S. J., Sluijs, A., Zeebe, R., Kump, L., Martindale, R. C., Greene, S. E., Kiessling, W., Ries, J., Zachos, J. C., Royer, D. L., Barker, S., Marchitto, T. M., Moyer, R., Pelejero, C., Ziveri, P., Foster, G. L., and Williams, B.: The geological record of ocean acidification, Science, 335, 1058–1063, doi:10.1126/science.1208277, 2012.

Hut, G.,: Consultants Group Meeting on Stable Isotope Reference Samples for Geochemical and Hydrological Investigations: Vienna, Austria, Report to Director General of the Institute of Atomic Energy Agency, 42 pp., 1987.

Kennett, J. P. and Stott, L. D.: Abrupt deep-sea warming, palaeoceanographic changes and benthic extinctions at the end of the Palaeocene, Nature, 353, 225–229, doi:10.1038/353225a0, 1991.

Kirtland Turner, S., Sexton, P. F., Charles, C. D., and Norris, R. D.: Persistence of carbon release events through the peak of early Eocene global warmth, Nat. Geosci., 12, 1–17, doi:10.1038/ngeo2240, 2014.

Kuiper, K. F., Deino, A., Hilgen, F. J., Krijgsman, W., Renne, P. R., and Wijbrans, J. R.: Synchronizing rock clocks of Earth history, Science, 320, 500–504, doi:10.1126/science.1154339, 2008.

Kurtz, A. C., Kump, L. R., Arthur, M. A., Zachos, J. C., and Paytan, A.: Early Cenozoic decoupling of the global carbon and sulfur cycles, Paleoceanography, 18, 1090, doi:10.1029/2003PA000908, 2003.

Laskar, J., Fienga, A., Gastineau, M., and Manche, H.: La2010: a new orbital solution for the long term motion of the Earth, Astron. Astrophys., 532, A89, doi:10.1051/0004-6361/201116836, 2011.

Liebrand, D., Lourens, L. J., Hodell, D. A., de Boer, B., van de Wal, R. S. W., and Pälike, H.: Antarctic ice sheet and oceanographic response to eccentricity forcing during the early Miocene, Clim. Past, 7, 869–880, doi:10.5194/cp-7-869-2011, 2011.

CPD
11, 1795–1820, 2015

Frequency, magnitude and character of hyperthermal events

V. Lauretano et al.

Littler, K., Röhl, U., Westerhold, T., and Zachos, J. C.: A high-resolution benthic stable-isotope record for the South Atlantic: implications for orbital-scale changes in Late Paleocene–Early Eocene climate and carbon cycling, Earth Planet. Sc. Lett., 401, 18–30, doi:10.1016/j.epsl.2014.05.054, 2014.

Lourens, L. J., Sluijs, A., Kroon, D., Zachos, J. C., Thomas, E., Röhl, U., Bowles, J., and Raffi, I.: Astronomical pacing of late Palaeocene to early Eocene global warming events, Nature, 435, 1083–1087, doi:10.1038/nature03814, 2005.

Lunt, D. J., Ridgwell, A., Sluijs, A., Zachos, J. C., Hunter, S., and Haywood, A.: A model for orbital pacing of methane hydrate destabilization during the Palaeogene, Nat. Geosci., 4, 775–778, doi:10.1038/ngeo1266, 2011.

McInerney, F. A., and Wing, S. L.: The Paleocene–Eocene thermal maximum: a perturbation of carbon cycle, climate, and biosphere with implications for the future, Annu. Rev. Earth Pl. Sc., 39, 489–516, doi:10.1146/annurev-earth-040610-133431, 2011.

Nicolo, M. J., Dickens, G. R., Hollis, C. J., and Zachos, J. C.: Multiple early Eocene hyperthermals: their sedimentary expression on the New Zealand continental margin and in the deep sea, Geology, 35, 699–702, doi:10.1130/G23648A.1, 2007.

Paillard, D., Labeyrie, L., and Yiou, P.: Macintosh program performs time-series analysis, Eos Trans. AGU, 77, 379, 1996.

Renne, P. R., Deino, A. L., Hilgen, F. J., Kuiper, K. F., Mark, D. F., Mitchell, W. S., Morgan, L. E., Mundil, R., and Smit, J.: Time scales of critical events around the Cretaceous–Paleogene boundary, Science, 339, 684–687, doi:10.1126/science.1230492, 2013.

Röhl, U., Westerhold, T., Monechi, S., Thomas, E., Zachos, J. C., Donner, B.: The Third and Final Early Eocene Thermal Maximum: Characteristics, Timing and Mechanisms of the “X” Event, GSA Annual Meeting 37, Geological Society of America, Salt Lake City, USA, 264 pp., 2005.

Sexton, P. F., Norris, R. D., Wilson, P. A., Pälike, H., Westerhold, T., Röhl, U., Bolton, C. T., and Gibbs, S.: Eocene global warming events driven by ventilation of oceanic dissolved organic carbon, Nature, 471, 349–352, doi:10.1038/nature09826, 2011.

Shackleton, N. J. and Hall, M. A.: The late Miocene stable isotope record, site 926, Proc. Ocean Drill. Program Sci. Results, 154, 367–373, doi:10.2973/odp.proc.sr.154.119.1997, 1997.

Slotnick, B. S., Dickens, G. R., Nicolo, M. J., Hollis, C. J., Crampton, J. S., Zachos, J. C., and Sluijs, A.: Large-amplitude variations in carbon cycling and terrestrial weathering during the

CPD
11, 1795–1820, 2015

latest Paleocene and earliest Eocene: the record at Mead Stream, New Zealand, J. Geol., 120, 487–505, doi:10.1086/666743, 2012.

Sluijs, A., Brinkhuis, H., Schouten, S., Bohaty, S. M., John, C. M., Zachos, J. C., Reichart, G.-J., Sinninghe Damsté, J. S., Crouch, E. M., and Dickens, G. R.: Environmental precursors to rapid light carbon injection at the Palaeocene/Eocene boundary, Nature, 450, 1218–1221, doi:10.1038/nature06400, 2007.

Stap, L., Sluijs, A., Thomas, E., and Lourens, L. J.: Patterns and magnitude of deep sea carbonate dissolution during Eocene Thermal Maximum 2 and H2, Walvis Ridge, southeastern Atlantic Ocean, Paleoceanography, 24, PA1211, doi:10.1029/2008PA001655, 2009.

Stap, L., Lourens, L. J., Thomas, E., Sluijs, A., Bohaty, S., and Zachos, J. C.: High-resolution deep-sea carbon and oxygen isotope records of Eocene Thermal Maximum 2 and H2, Geology, 38, 607–610, doi:10.1130/G30777.1, 2010.

Thomas, E. and Shackleton, N. J.: The Paleocene–Eocene benthic foraminiferal extinction and stable isotope anomalies, Geol. Soc. London, Spec. Publ., 101, 401–441, doi:10.1144/GSL.SP.1996.101.01.20, 1996.

Westerhold, T. and Röhl, U.: High resolution cyclostratigraphy of the early Eocene – new insights into the origin of the Cenozoic cooling trend, Clim. Past, 5, 309–327, doi:10.5194/cp-5-309-2009, 2009.

Westerhold, T., Röhl, U., Laskar, J., Raffi, I., Bowles, J., Lourens, L. J., and Zachos, J. C.: On the duration of magnetochrons C24r and C25n and the timing of early Eocene global warming events: implications from the Ocean Drilling Program Leg 208 Walvis Ridge depth transect, Paleoceanography, 22, PA2201, doi:10.1029/2006PA001322, 2007.

Westerhold, T., Röhl, U., Raffi, I., Fornaciari, E., Monechi, S., Reale, V., Bowles, J., and Evans, H. F.: Astronomical calibration of the Paleocene time, Palaeogeogr. Palaeocl., 257, 377–403, doi:10.1016/j.palaeo.2007.09.016, 2008.

Zachos, J. C., Pagani, M., Sloan, L., Thomas, E., and Billups, K.: Trends, rhythms, and aberrations in global climate 65 Ma to present, Science, 292, 686–693, 2001.

Zachos, J. C., Kroon, D., and Blum, P.: ODP Leg 208: the early Cenozoic extreme climates transect along walvis ridge, in: Proceedings of the Ocean Drilling Program Initial Reports, 208, 2004.

Zachos, J. C., Röhl, U., Schellenberg, S. A., Sluijs, A., Hodell, D. A., Kelly, D. C., Thomas, E., Nicolo, M., Raffi, I., Lourens, L. J., McCarren, H., and Kroon, D.: Rapid acidification of

CPD
11, 1795–1820, 2015

the ocean during the Paleocene–Eocene thermal maximum, Science, 308, 1611–1615, doi:10.1126/science.1109004, 2005.
Zachos, J. C., Dickens, G. R., and Zeebe, R. E.: An early Cenozoic perspective on greenhouse warming and carbon-cycle dynamics, Nature, 451, 279–283, doi:10.1038/nature06588, 2008.
Zachos, J. C., McCarren, H., Murphy, B., Röhl, U., and Westerhold, T.: Tempo and scale of late Paleocene and early Eocene carbon isotope cycles: implications for the origin of hyperthermals, Earth Planet. Sc. Lett., 299, 242–249, doi:10.1016/j.epsl.2010.09.004, 2010.
Zeebe, R. E. and Zachos, J. C.: Long-term legacy of massive carbon input to the Earth system: Anthropocene vs. Eocene., Philos. T. R. Soc. A., 371, 20120006, doi:10.1098/rsta.2012.0006, 2013.

CPD
11, 1795–1820, 2015

Table 1. Age-depth tie points based on the tuning of the filtered 3 m-period extracted from Site 1262 color reflectance record and the long eccentricity cycle extracted from the Laskar solution La2010d (Laskar et al., 2011).

Site 1262 3 m period filter	Long eccentricity cycle (kyrs) Laskar 2010d (Option 1)	Long eccentricity cycle (kyrs) Laskar 2010d (Option 2)
102.750	51 800	52 206
104.231	52 003	52 410
105.711	52 206	52 614
107.167	52 410	52 816
108.648	52 614	53 017
110.129	52 816	53 216
111.635	53 017	53 415
113.193	53 216	53 615
114.750	53 415	53 815
116.359	53 615	54 016
117.865	53 815	54 218

CPD
11, 1795–1820, 2015

Table 2. Color reflectance tie points from ODP Site 1263 and Site 1262 and interpolated ages obtained from the astronomically tuned age model.

Samples	Site 1263 Depth (mbsf)	Site 1263 Depth (mcd)	Samples	Site 1262 Depth (mbsf)	Site 1262 Depth (mcd)	Interpolated Age (Ma) Option 1	Interpolated Age (Ma) Option 2
1263A-26H-4, 147.5	228.575	265.425	1262B-11H-4, 137.5	92.275	101.855	51.610	52.014
1263A-26H-5, 50	229.1	265.95	1262B-11H-5, 42.5	92.825	102.405	51.727	52.132
1263A-26H-5, 90	229.5	266.35	1262B-11H-5, 102.5	93.425	103.005	51.835	52.241
1263A-26H-5, 115	229.75	266.6	1262B-11H-5, 137.5	93.775	103.355	51.883	52.289
1263A-26H-6, 147.5	231.575	268.425	1262B-11H-6, 45	94.35	103.93	51.962	52.369
1263A-26H-7, 30	231.9	268.75	1262A-10H-2, 120	88.2	104.31	52.014	52.421
1263B-22H-5, 100	230.9	269.23	1262A-10H-2, 145	88.45	104.56	52.048	52.455
1263B-22H-5, 125	231.15	269.48	1262A-10H-3, 20	88.7	104.81	52.082	52.490
1263B-22H-6, 142.5	232.825	271.155	1262A-10H-3, 60	89.1	105.21	52.137	52.545
1263B-22H-7, 45	233.35	271.68	1262A-10H-3, 87.5	89.375	105.485	52.175	52.583
1263A-27H-1, 65	232.75	272.78	1262A-10H-4, 2.5	90.025	106.135	52.265	52.673
1263A-27H-2, 7.5	233.675	273.705	1262A-10H-4, 27.5	90.275	106.385	52.300	52.707
1263A-27H-2, 17.5	233.775	273.805	1262A-10H-4, 37.5	90.375	106.485	52.314	52.721
1263A-27H-2, 25	233.85	273.88	1262A-10H-4, 45	90.45	106.56	52.325	52.732
1263A-27H-2, 125	234.85	274.88	1262A-10H-4, 77.5	90.775	106.885	52.370	52.777
1263A-27H-2, 145	235.05	275.08	1262B-12H-1, 70	96.6	107.24	52.420	52.826
1263A-27H-3, 40	235.5	275.53	1262B-12H-1, 85	96.75	107.39	52.441	52.846
1263A-27H-3, 67.5	235.775	275.805	1262B-12H-1, 100	96.9	107.54	52.461	52.867
1263A-27H-3, 100	236.1	276.13	1262B-12H-1, 110	97	107.64	52.475	52.880
1263A-27H-3, 135	236.45	276.48	1262B-12H-1, 120	97.1	107.74	52.489	52.894
1263A-27H-4, 77.5	237.375	277.405	1262B-12H-2, 5	97.45	108.09	52.537	52.941
1263A-27H-4, 100	237.6	277.63	1262B-12H-2, 22.5	97.625	108.265	52.561	52.965
1263A-27H-4, 137.5	237.975	278.005	1262B-12H-2, 60	98	108.64	52.613	53.016
1263A-27H-5, 70	238.8	278.83	1262B-12H-2, 110	98.5	109.14	52.681	53.083
1263C-9H-4, 105	240.45	280.24	1262B-12H-2, 135	98.75	109.39	52.715	53.117
1263C-9H-5, 15	241.05	280.84	1262B-12H-3, 12.5	99.025	109.665	52.753	53.154
1263C-9H-5, 100	241.9	281.69	1262B-12H-3, 40	99.3	109.94	52.790	53.191
1263C-9H-6, 2.5	242.425	282.215	1262B-12H-3, 57.5	99.475	110.115	52.814	53.214
1263C-9H-6, 15	242.55	282.34	1262B-12H-3, 65	99.55	110.19	52.824	53.224
1263C-9H-6, 32.5	242.725	282.515	1262B-12H-3, 85	99.75	110.39	52.851	53.251
1263C-9H-6, 82.5	243.225	283.015	1262B-12H-4, 10	100.5	111.14	52.951	53.350
1263A-28H-1, 40	242	284.52	1262B-12H-4, 65	101.05	111.69	53.024	53.422
1263A-28H-1, 95	242.55	285.07	1262B-12H-4, 122.5	101.625	112.265	53.097	53.496
1263A-28H-1, 115	242.75	285.27	1262A-11H-1, 137.5	96.375	112.425	53.118	53.516
1263A-28H-2, 40	243.5	286.02	1262A-11H-2, 2.5	96.525	112.575	53.137	53.536
1263A-28H-2, 70	243.8	286.32	1262A-11H-2, 12.5	96.625	112.675	53.150	53.549
1263A-28H-2, 107.5	244.175	286.695	1262A-11H-2, 50	97	113.05	53.198	53.597
1263A-28H-3, 5	244.65	287.17	1262A-11H-2, 67.5	97.175	113.225	53.220	53.619
1263A-28H-3, 27.5	244.875	287.395	1262A-11H-2, 80	97.3	113.35	53.236	53.635
1263A-28H-3, 32.5	244.925	287.445	1262A-11H-2, 85	97.35	113.4	53.243	53.642
1263A-28H-3, 65	245.25	287.77	1262A-11H-2, 97.5	97.475	113.525	53.258	53.658
1263A-28H-3, 70	245.3	287.82	1262A-11H-2, 105	97.55	113.6	53.268	53.667
1263B-24H-2, 147.5	245.875	288.165	1262A-11H-2, 132.5	97.825	113.875	53.303	53.703
1263B-24H-3, 67.5	246.575	288.865	1262A-11H-2, 147.5	97.975	114.025	53.322	53.722
1263B-24H-4, 135	248.75	291.04	1262A-11H-3, 95	98.95	115	53.446	53.846
1263B-24H-5, 47.5	249.375	291.665	1262A-11H-3, 145	99.45	115.5	53.508	53.909
1263B-24H-6, 20	250.6	292.89	1262A-11H-4, 52.5	100.025	116.075	53.580	53.981
1263C-10H-5, 65	251.05	292.93	1262A-11H-4, 57.5	100.075	116.125	53.586	53.987
1263C-10H-5, 82.5	251.225	293.105	1262A-11H-4, 72.5	100.225	116.275	53.605	54.006
1263C-10H-5, 110	251.5	293.38	1262A-11H-4, 87.5	100.375	116.425	53.624	54.025
1263C-10H-7, 1	252.91	294.79	1262A-11H-4, 135	100.85	116.9	53.687	54.089
1263C-10H-7, 5	252.95	294.83	1262A-11H-5, 5	101.05	117.1	53.713	54.089
1263C-10H-7, 10	253	294.88	1262A-11H-5, 10	101.1	117.15	53.720	54.122

CPD
11, 1795–1820, 2015

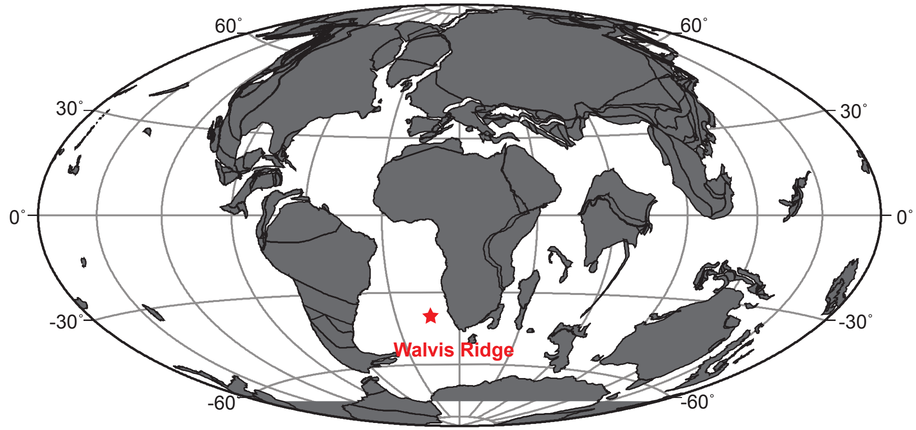

Figure 1. Paleogeographic reconstruction for the early Eocene (∼ 55 Ma) showing the position of Walvis Ridge Sites at (map generated at http://www.odsn.de/odsn/services/paleomap/paleomap.html, modified).

CPD
11, 1795–1820, 2015

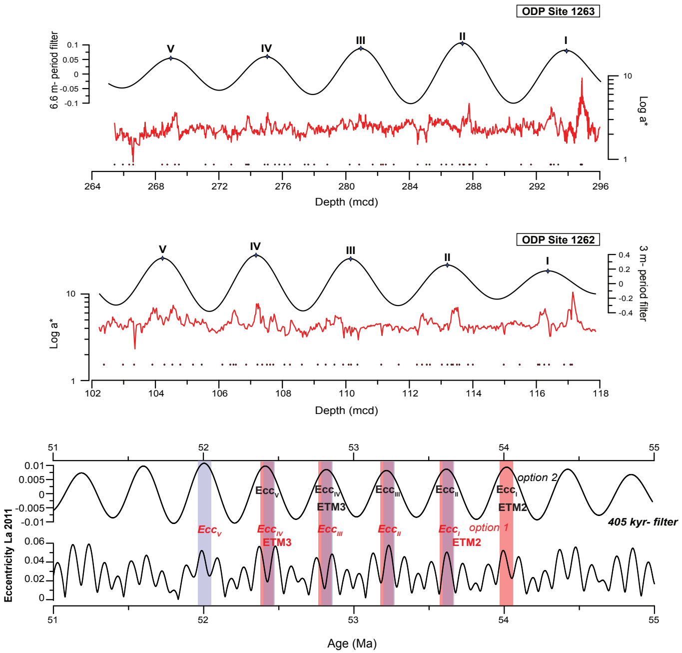

Figure 2. The floating orbitally-tuned age model was constructed based on the red over green color ratio (a*) records of ODP Sites 1263 and 1262. The extracted ∼ 3 m period from Site 1262 was used to tune the record to the extracted 405 kyr eccentricity component of the La2010d orbital solution (Laskar et al., 2011), with maximum a* values corresponding to maximum eccentricity values. Interpolated ages were transferred then to Site 1263 by using age-depth tie points (black dots). Uncertainties in dating proxies prevent an absolute age for this time interval, anchored to the lack of an absolute age for the PETM. Therefore, different tuning options are available within an 800 kyr window (Westerhold et al., 2008). Two possible options are shown.

CPD
11, 1795–1820, 2015

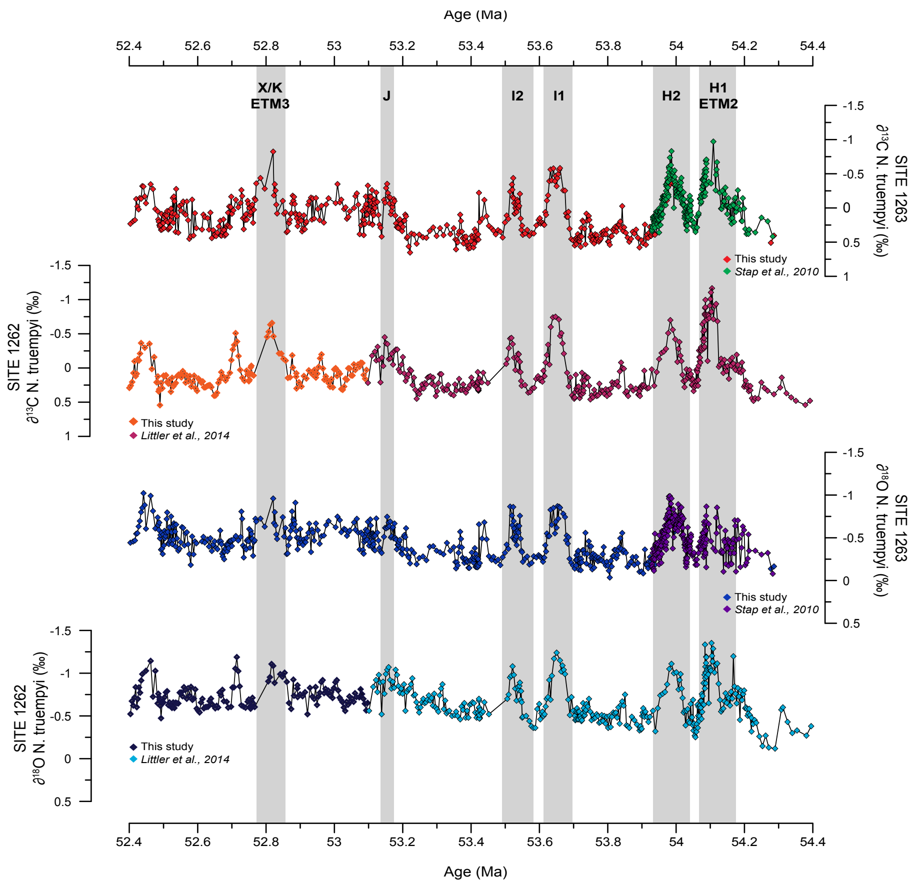

Figure 3. Benthic *N. truempyi* $\delta^{13}C$ and $\delta^{18}O$ records from Site 1263 and Site 1262, plotted vs. Age (Ma), (option 2- Westerhold et al., 2008). Highlighted intervals represent the position of the early Eocene hyperthermal events.

CPD
11, 1795–1820, 2015

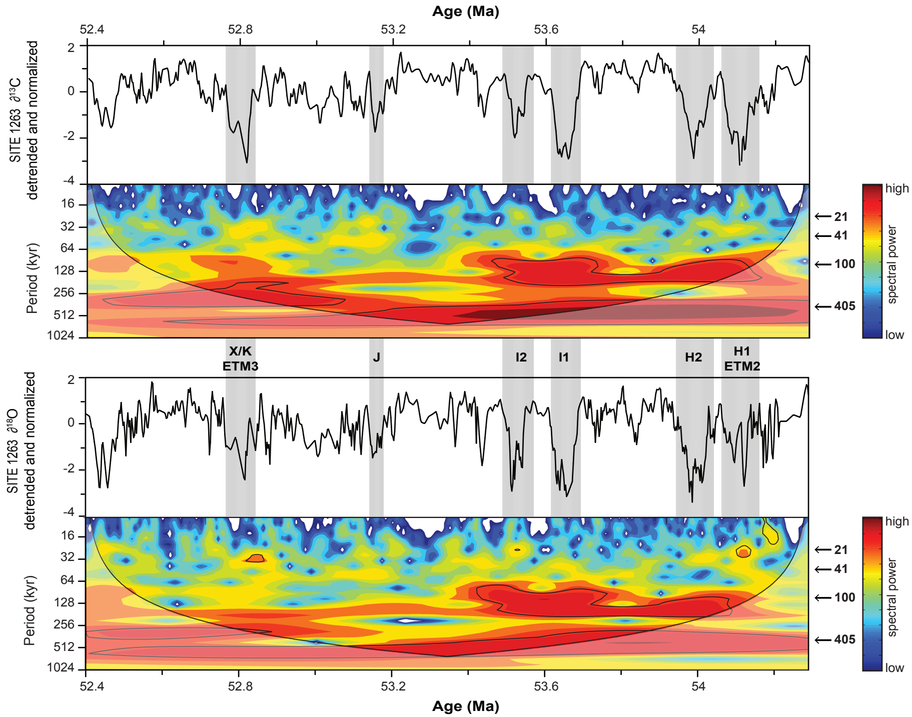

Figure 4. Evolutionary wavelet analyses for $\delta^{13}C$ and $\delta^{18}O$ were performed using a Morlet mother wavelet of an order of 6. The shaded area represents the 95 % significance level. Spectral power above the confidence level is concentrated at distinct frequencies, corresponding to the long 405 kyr and short eccentricity 100 kyr cycles. Highlighted intervals represent the position of the early Eocene hyperthermal events.

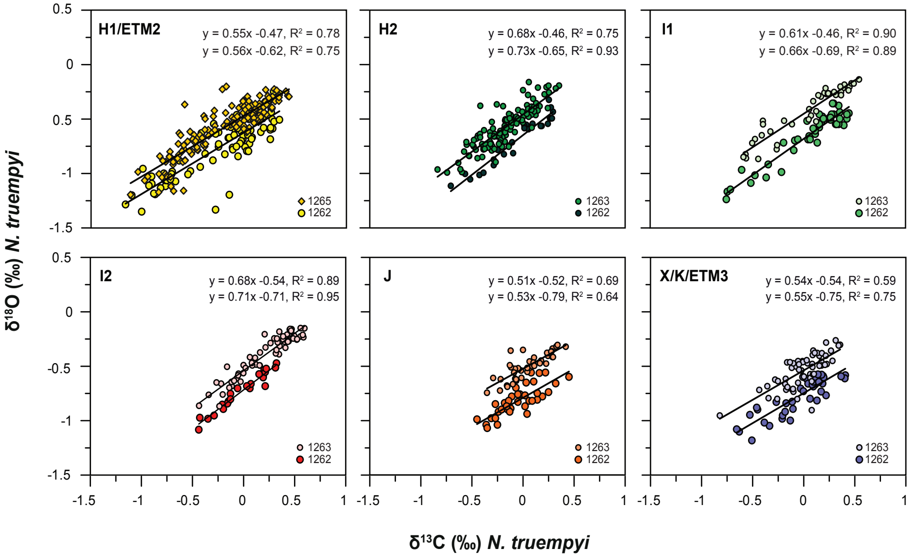

Figure 5. Relationship between the oxygen and carbon isotope values of *N. truempyi* during ETM2, H2, I1, I2, J and ETM3/X in Site 1263 and Site 1262. Data for ETM2 and H2 from Stap et al. (2010) and for I1, I2 and J at Site 1262 from Littler et al. (2014). Note that, because of intense dissolution at Site 1263, ETM2 data were chosen from Site 1265. For all the events, throughout the entire event (onset + recovery phases), changes in the exogenic carbon pool are linearly related to warming. Linear regression equations refer to Site 1263 (top) and Site 1262 (bottom), respectively.

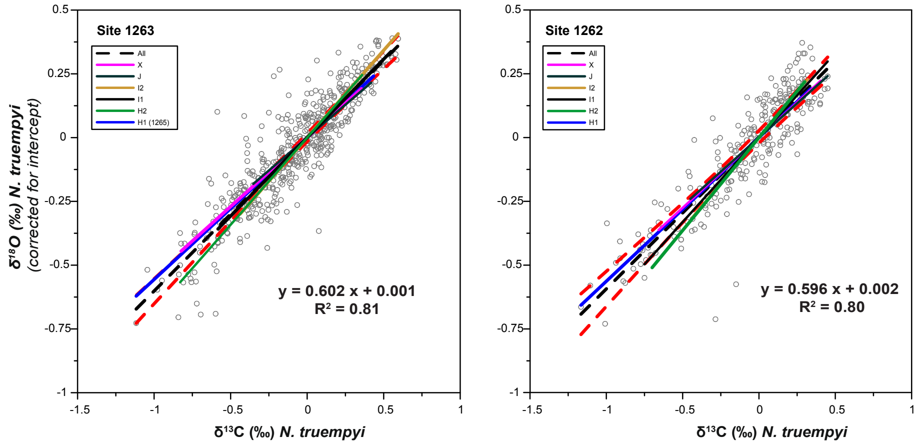

Figure 6. Slope of each event plotted together with the average slope (from all the events). The red dashed line indicates the 99 % confidence interval.

CPD
11, 1795–1820, 2015

Frequency, magnitude and character of hyperthermal events

V. Lauretano et al.